NURC TIME SERIES STIMULATOR BENCHMARK FOR WESTON SONAR SCENARIO A2

KD LePage, NATO Undersea Research Centre, Viale San Bartolomeo 400, 19126 La Spezia (SP) Italy

1 INTRODUCTION

The simulation of element-level reverberation and target returns on line arrays is addressed for real-time in-the-loop active ASW stimulation applications. Simulation of element level pressure time series for bistatic geometries at mid frequencies (1-5 kHz) is fairly straightforward for targets but extremely challenging for reverberation. Reverberation is challenging because it entails the superposition of an extremely large number of target returns from individual environmental scatterers on the boundaries of the waveguide. Real-time reverberation simulation approaches based on such a summation are doomed to computational inefficiency due to the overwhelming large number of scatterers that contribute to bistatic reverberation seen at the element level. While increasing bandwidth reduces the number of scatterers contributing to the reverberation to some degree, multipath spread tends to limit the advantage gained, and in any case the reverberation received at the individual elements must be summed over the full azimuthal dimension of the scatterers.

The solution lies in the use of simplified closed form expressions for the bistatic reverberation intensity that have recently been developed at NURC. These expressions are used to determine the wavenumber domain intensity on a straight array as a function of time. The (slow) time-varying intensity as a function of wavenumber is sufficient to rapidly compute reverberation pressure time series at the element level with realistic statistical characteristics.

In this article the theory for the fast reverberation and target simulation is developed and an algorithm for the computation of element level time series on a horizontal line array is presented. Results show that the algorithm is capable of computing element level time series for bistatic mid frequency sonar in real-time.

2 BACKGROUND

2.1 Reverberation Stimulation

The simulation of realistic mid-frequency bistatic active reverberation time series for real-time applications is of much current interest. Applications such as operator training, system dry bench testing, signal processing algorithm development and sonar robotics development all require accurate, fast simulations of reverberation for MCM and ASW scenarios. At NURC, the collaborative ASW project has need for a real-time stimulation capability for the evaluation of on-board signal processing and autonomy algorithms for autonomous underwater vehicles [1-3]. But the real-time computation of reverberation is a very demanding task. More than propagation alone, more than scattering, reverberation is a combination of both with a large number of contributing terms. ASW areas of interest typically encompass areas of tens to hundreds of kilometres squared, while wavelengths are typically much less than a meter. Add to this the complexity of multipath propagation to and from all the contributing scatterers, and it is easily perceived that the most straight-forward simulation approaches are doomed to failure. For instance, if one proceeds along the lines of reasoning that several scatterers per square wavelength should be laid down onto the sea surface or bottom of the simulation environment, and that the impulse responses from all these scatterers should be summed to create the reverberation time series, the computational demands quickly become untenable with ray theory for ranges corresponding to more than a few water depths, or with modes at most frequencies of interest. If on the other hand, one wishes to use reverberation covariance theories to generate the reverberation using Cholesky or eigenvalue decomposition (which limits the number of synthesis terms to the number of receiver elements), one runs the risk of becoming overwhelmed by the number of frequencies required for Fourier synthesis, even assuming one is able to resolve thorny issues of how to interpolate the covariance eigenvalues and eigenvectors which for reverberation evolve as a function of time.

2.1.1 Proposed Approach

The approach proposed to overcome the challenges outlined above is to re-derive the very rapidly computed bistatic reverberation intensity formulae of Harrison [4], but leaving the received intensity as a decomposition in both azimuth and grazing angle at the receiver. The second step is to assume a straight array with uniform phone spacing at the receiver. In the case of a uniformly sampled straight line array deployed at a constant depth, the intensity resolution of the array is composed of N+1 discrete wavenumbers at the sample frequency (N+1 because forward and aft endfire are indistinguishable), allowing the summation of the conical beam pattern of a uniformly shaded array across the time evolving azimuth-grazing angle distribution of the scattered intensity. Each of these products produces a time-dependent intensity in each of the N+1 wavenumbers resolved by the array. It then remains to take the square root of each of these intensities, interpolate in time to the sample frequency desired of the stimulator, define a frequency envelope function consistent with the source waveform, and randomize each of the quadratures of the resulting complex envelope. The resulting complex time series are summed for each receiver over the N+1 wavenumbers, and the pressure is obtained by taking the real part.

2.1.2 Limitations

As opposed to the sum of the impulse response from a large number of scatterers, such an approach is extremely efficient, as there are only N+1 randomized waveforms that need to be added together to simulate the reverberation. The limitations are 1) that the array is assumed to be operating at or near the design frequency (although with the proper shifting of the conical beampatterns over the time evolution of the azimuth and grazing angle decomposed reverberation intensity this restriction may be relaxed), 2) that the array is straight, deployed at a single depth, and uniformly sampled in space (the first two of these assumptions are the most restrictive), and 3) that the scatterers are homogeneously distributed and that inter-ping correlations of reverberation originating from the same piece of the bottom are not required, as for example with providing stimulation for synthetic aperture sonar processing, or when simulating prominent bottom scatterers for later imaging. Compared to Cholesky or eigenvalue decomposition of an expression of the reverberation covariance, the approach is unable to handle the general case of a dangling or curved array.

2.2 Target and Direct Blast Stimulation

As opposed to the stimulation of reverberation, the computation of time series scattered by an object, even at long range and at mid frequencies, is not too computationally demanding, as long as multiple scattering effects are neglected. Multiple scattering effects account for the re-excitation of the target (or the scatterers, if it is to be included in the reverberation calculation) by waves that have already reflected from the target but have been re-directed by the waveguide to become incident energy. The most common effect are multiples from the bottom or free surface of non-specularly scattered energy from the target re-exciting the target, creating an extended late-time response. Another important effect is multiple scattering on the target itself: targets can create forward scattered energy which when added to the incident field, creates shadows that may prevent other parts of the target from being illuminated. A common example of this is that the back side of a target is generally not considered to be illuminated when using for example the Kirchhoff approximation. Finally, forward scattered energy combined with the incident field forms deep shadows on scatterers behind the target at very high ka. These shadows are extremely important for target classification for high frequency (> 50kHz) mine countermeasure systems, but are not commonly seen or exploited by traditional mid-frequency ASW systems.

3 STIMULATOR THEORY

3.1 Reverberation

Reverberation is the summation of many acoustic returns from the natural distribution of scatterers in the environment. Generally little is known about the individual scatterers, although in some cases an environmental survey has been conducted to statistically characterize them (such as obtaining an estimate of the bottom roughness spectrum), or to provide measurements of environmental drivers such as wind speed which may be used to indirectly estimate the free-surface roughness spectrum. If bottom or free-surface roughness spectra are known then they may be used as input to theories used to predict a scattering function for these surfaces; alternatively these scattering functions may be estimated from reverberation or scattering data themselves. In any case the scattering functions, which are expressed as a ratio of scattered intensity at an output grazing angle to incident intensity at

an input grazing angle for a given bistatic angle, are a function of frequency and the roughness characteristics of the boundaries.

The scatterers are viewed through the lens of the ocean acoustics. For deep water the characteristics of this lens are largely determined by the variable index of refraction of the ocean caused by inhomogeneities in the temperature, salinity and density that affect the acoustic sound speed through the equations of state. These properties are to a large degree horizontally stratified, so that the greatest changes occur as a function of depth. As the acoustic propagation of interest for sonar is also horizontally directed, the gradients across acoustic wavefronts are at their maximum, and strong bending of these wavefronts may occur, leading to shadow zones and interesting structures in acoustic travel time. In shallow water these effects are strongly modulated by interactions with the bottom and the surface, both of which introduce frequency and angle dependent reflection loss, with smaller angles being favoured by lower loss.

Together the pieces described above, frequency and angle selective propagation to a number of scatterers, which are characterized by a scattering function that re-directs scattered intensity towards a receiver, with additional angle and frequency dependent propagation being suffered on the way, are the traditional view of reverberation and characterizes the reverberation intensity, which is expressed as a function of travel time and azimuthal angle from a notional horizontal receiving array. For an element level stimulator two transformations of this characterization are required: first, the acoustic intensity as a function of horizontal azimuth must be summed across all azimuths on each receiver, and second, the square root of this intensity must be obtained and convolved with the source waveform, all while retaining the correct phase relationship between neighbouring elements so that the elements produce beam-time series consistent with the original intensity distribution in time and azimuth.

Of these two transformations, the most computationally demanding is the transformation to the fast time domain of the azimuthally summed intensity, since this requires up-sampling to the sample frequency of the data acquisition system that is being emulated. Furthermore, since the elements form an array with horizontal resolving power, the azimuthal summation of the bistatic reverberation intensity must be performed *N+1* times, where *N* is the number of elements in the array and therefore the number of horizontal wavenumbers resolved by the array. The details are given below.

3.1.1 Simple expressions for the time and angular evolution of bistatic reverberation intensity

The effects of multiple boundary interactions on the propagation to and from the scatterers are very simply accounted for in the ray-averaged approach of Weston and Harrison [4]. In the absence of refractive effects (isovelocity waveguide in shallow water) the incident intensity (one half of the total intensity) at the range of the scatterers is well approximated by

$$I(r_1) = \frac{I_S}{rH} \int_0^{\pi/2} \left|R(\theta)\right|^{r_1 \tan\theta / H} d\theta \tag{1}$$

where I_S is the radiated source intensity at 1 m in μPa, $\boldsymbol{r}_s$ is the source location, $\boldsymbol{r}_{scat}$ is the scatterer location, $r_1 = |\boldsymbol{r}_s - \boldsymbol{r}_{scat}|$ is the range from the source to the scatterer, H is the (range independent) water depth, $R(\theta)$ is the (pressure) reflection loss as a function of grazing angle θ, and the power to which the square of the absolute value of R is raised is equal to the number of boundary interactions in a given range for a ray path with grazing angle θ. Using a similar expression for the intensity at the receiver location due to a source at the scatterer location, and allowing for an angular dependent scattering strength, the reverberation intensity is

$$I_{rev}(r_1, r_2) = \frac{I_S}{r_1 r_2 H^2} \int_0^{\pi/2} d\theta_1 \int_0^{\pi/2} d\theta_2 \left|R(\theta_1)\right|^{r_1 \tan\theta / H} ss(\theta_1, \theta_2, \Theta) A(r_1, r_2, \Theta) \left|R(\theta_2)\right|^{r_2 \tan\theta / H} \tag{2}$$

where $\boldsymbol{r}_{rec}$ is the receiver location, $r_2 = |\boldsymbol{r}_{rec} - \boldsymbol{r}_{scat}|$ is the range from the source to the scatterer, and Θ is the bistatic angle $\cos^{-1}(\boldsymbol{e}_1 \cdot \boldsymbol{e}_2)$ where $\boldsymbol{e}_1$ is the unit vector from the scattering patch to the source $\boldsymbol{e}_1 = (\boldsymbol{r}_s - \boldsymbol{r}_{scat})/r_1$ and $\boldsymbol{e}_2$ is the unit vector from the scattering patch to the receiver $\boldsymbol{e}_2 = (\boldsymbol{r}_{rec} - \boldsymbol{r}_{scat})/r_2$. The scattering coefficient *ss* is defined as

$$ss(\theta_1,\theta_2,|\phi_2-\phi_1|) \equiv 10^{SS/10} = \lim_{r_2\to\infty} \frac{I_s(\theta_2,\phi_2)r_2^2}{I_i(\theta_1,\phi_1)A} \quad (3)$$

where SS is the scattering strength in dB, and I_i is the intensity of a plane wave at grazing angle θ_1 on a scattering surface of area A, I_s is the far field scattered intensity from this surface at range r_2, and the scattering into bistatic angles $\phi_2-\phi_1$ is generally assumed to be homogeneous in bistatic angle.

The area of the scattering patch $A(r_1, r_2, \Theta)$ in (2) is defined in bistatic geometry as [4]

$$A(r_1,r_2,\Theta) = \delta t \delta\phi \frac{2cr_1r_2^2}{(ct)^2-L^2} \quad (4)$$

where c is the speed of sound in the ocean, t is the total time $t = (r_1 + r_2)/c$, L is the source-receiver separation $L=|r_{rec} - r_s|$, and δt and $\delta\phi$ are the temporal duration of the (pulse compressed) signal and the angular resolution of the array at the receiver location pointing in the direction of the bottom scattering patch.

To convert (2) to an explicit expression in time for reverberation intensity requires that we be able to express r_1, r_2 and Θ in terms of t, L and the angle ϕ from the source-receiver axis to the scattering patch as shown in Fig. 1

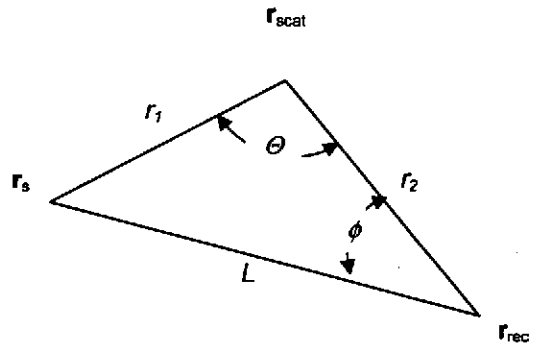

Figure 1: Bistatic reverberation geometry

The needed expressions are given in [4] as

$$r_1(t,\phi) = \frac{(ct)^2 + L^2 - 2Lct\cos\phi}{2(ct - L\cos\phi)} \quad (5)$$

$$r_2(t,\phi) = \frac{(ct)^2 - L^2}{2(ct - L\cos\phi)} \quad (6)$$

and

$$\Theta = a\cos\left(\frac{2(ct - L\cos\phi)^2}{(ct)^2 + L^2 - 2Lct\cos\phi} - 1\right) \quad 7)$$

Eq. (2) may be integrated over grazing angle if the form of scattering function is known. In the case of the well known and sometimes representative Lambert's law this form is [5]

$$SS = 10^{-\mu/10} \sin(\theta_1)\sin(\theta_2) \tag{8}$$

Since horizontal line arrays do not have the ability to resolve over grazing angle independently of azimuth, it is only appropriate to perform the integral over the incident field grazing angle θ_1 in (2), and apply the array response before integrating over the receiver grazing angles. This may be done in closed form if one also uses the log-linear approximation for the reflection coefficient R

$$\left|R(\theta)\right|^2 \approx \exp(-\alpha\theta) \tag{9}$$

where

$$\begin{aligned} \alpha &= -\left.\frac{\partial \ln\left(\left|R(\theta)\right|^2\right)}{\partial\theta}\right|_{\theta=0} && \theta \le \theta_c \\ &= \infty && \theta > \theta_c \end{aligned} \tag{10}$$

in which case, using (8) and assuming θ_1, θ_2 small, the θ_1, θ_2 integrals in (2) are separable and (2) may be written

$$\begin{aligned} I_{rev} &= I_S \frac{10^{-\mu/10}}{r_1 r_2 H^2} A(r_1, r_2, \Theta)\left(\int_0^{\theta_c} \theta_1 e^{-\alpha\theta_1^2 r_1/2H} d\theta_1\right)\int_{-\theta_c}^{\theta_c} \theta_2 e^{-\alpha\theta_2^2 r_2/2H} d\theta_2 \\ &= I_S \frac{10^{-\mu/10}}{\alpha r_1^2 r_2 H} A(r_1, r_2, \Theta)\left(1-\exp\left(-\alpha\theta_c^2 r_1/2H\right)\right)\int_{-\theta_c}^{\theta_c} \theta e^{-\alpha\theta^2 r_2/2H} d\theta \end{aligned} \tag{11}$$

Using (5), (6) and (7), (11) may be evaluated as a function of time t and angle from the receiver-source axis ϕ to yield the reverberation intensity as a function of time, azimuth and grazing angle at the receiver $I(t, \phi, \theta)$

$$I_{rev}(t,\theta,\phi) = S\frac{10^{-\mu}}{\alpha r_1^2 r_2 H} A(t,\phi)\left(1-\exp\left(-\alpha\theta_c^2 r_1(t,\phi)_1/2H\right)\right)\theta\exp\left(\alpha\theta^2 r_2(t,\phi)/2H\right) \tag{12}$$

In the stimulator implementation, (2) using (4) through (8) are used in lieu of (12). This improves accuracy by using the true reflection coefficient as a function of grazing angle rather than the log-linear approximation.

3.2 Target

The return from a target is in many ways a much simpler calculation than bistatic reverberation, if only for the fact that reverberation is the sum of many small scattering events, each of which may be thought of as a target. However, targets have complicating characteristics of their own, the most important of which are potentially large size with respect to a wavelength, and velocity. The first feature, large size, means that the target scattering response may be highly directive, not only in the forward scattering regime where the scattered field combines with the incident field to form a shadow, but also into specular angles which may be in a backscattered direction of significance to the sonar performance. The second feature, target velocity, introduces time dilation or contraction of the scattered waveform depending on source-target-receiver geometry. For geometries where the sum of the inner product of the pointing vectors from the target to the source and receiver with the target velocity vector is negative, a downward shift of the ensonifying frequency is found in the scattered field. For opposite geometries, the scattered field is compressed in time, leading to an upward shift in the frequency content. Shifts in the frequency of an acoustic field introduced by source, receiver or target motion are called Doppler shifts.

3.2.1 One-way impulse response of a shallow water waveguide

The target is assumed to be a sphere with zero velocity. While such a target may be large, the assumption at this point is that it has zero Doppler. Most of the complexity of the response is therefore in the Greens functions from the source to the target, and from the target to the receiver. For one-way propagation in shallow water a convenient form for computing these Greens functions is to use a normal mode expansion

$$p(\omega, \mathbf{r}_s, z_s | \mathbf{r}_{tar}, z_{tar}) = \sqrt{\frac{2\pi}{r_1}} \sum_{n=1}^{N} \frac{\psi(\omega, z_s)\psi(\omega, z_{tar})}{\sqrt{k_m}} \exp(ik_m(\omega) r_1) \tag{13}$$

where the mode shape functions ψ are functions of frequency and depend on depth only in range independent environments, and they together with the horizontal wavenumbers k_{nr} satisfy the depth-separated Helmholtz equation

$$\left(\frac{\partial^2}{\partial z^2} + \frac{\omega^2}{c^2(z)}\right)\psi_n(\omega) = k_{nr}^2(\omega)\psi_n(\omega). \tag{14}$$

Many codes are available for the rapid computation of the mode shape functions and wavenumbers [5,6]. Notice that in comparison with (1), Eq. (13) is explicitly frequency dependent and that generally the number of modes increases linearly with frequency. The frequency dependence of (1) is subsumed into the reflection coefficient, and the number of modes is assumed to be infinite. Another important distinction is that (1) is valid only for waveguides where the speed of sound is independent of depth, while mode shapes and wavenumbers that satisfy (14) can generally be found for all realistic sound speed profiles $c(z)$.

The implication of (13) being in the frequency domain is that it must be Fourier transformed to obtain the impulse response of the shallow water waveguide. Eq. (1) on the other hand, already being an expression for intensity and having a kernel which depends only on range and angle, cannot be Fourier transformed to obtain an time domain expression. Instead grazing angle must be converted to slant range, and all ranges converted to time based on straight ray-paths [7]. The equivalent expression for the evolution of the intensity in the time domain is then

$$I(\tau)d\tau = \frac{2}{rH}\sqrt{\frac{c}{2r\tau}}\left|R\left(\sqrt{2c\tau/r}\right)\right|^{\sqrt{\frac{2\tau r}{t_H H}}} d\tau \tag{15}$$

where $\tau = t - r_1/c$ and $t_H = H/c$. Equation (15) is obtained from (7) in [7] using the substitutions $|R(\theta)|^2 \approx \exp(-\alpha\theta)$ and $\theta^2 \approx 2c\tau/r$.

While the square root of (15) could be used as a basis to estimate the impulse response of the channel, we instead take advantage of the relative insensitivity of the mode shapes ψ to frequency to allow expansion of the wavenumber about the centre frequency

$$\begin{aligned} p(t, \mathbf{r}_s, z_s | \mathbf{r}_{tar}, z_{tar}) &\approx \sqrt{\frac{2\pi}{r_1}} \sum_{n=1}^{N} \frac{\psi(\omega_o, z_s)\psi(\omega_o, z_{tar})}{\sqrt{k_m^o}} \int_{-\infty}^{\infty} s(\omega) \exp\left(-i\left(\omega t - k_m(\omega) r_1\right)\right) d\omega \\ &\approx \sqrt{\frac{2\pi}{r_1}} \sum_{n=1}^{N} \frac{\psi(\omega_o, z_s)\psi(\omega_o, z_{tar})}{\sqrt{k_m^o}} \exp\left(-i\left(\omega_o t - k_m^o r_1\right)\right) \\ &\quad \times \frac{1}{2\pi} \int_{-\infty}^{\infty} s(\omega - \omega_o) \exp\left(-i\left(\omega\left(t - \frac{\partial k_m}{\partial \omega} r_1\right) - \frac{\omega^2}{2}\frac{\partial^2 k_m}{\partial \omega^2} r_1\right)\right) d\omega \end{aligned} \tag{16}$$

For source spectra which have an exponential form, such as

$$s(\omega)=\begin{cases} S(\omega_o) & uniform \\ S(\omega_o)\exp\left(-\omega^2/2\Delta\omega^2\right) & Gaussian, \\ S(\omega_o)\exp\left(-\omega^2 T/i2(\omega_1-\omega_2)\right) & LFM \end{cases} \tag{17}$$

the frequency integral in (16) is analytically integrable, which yields the narrowband approximation for the channel impulse response in the modal basis

$$\begin{aligned} p\left(t,\mathbf{r}_s,z_s\middle|\mathbf{r}_{tar},z_{tar}\right) \approx \frac{S(\omega_o)}{2\pi}\sqrt{\frac{2\pi}{r_1}}\sum_{n=1}^{N}\frac{\psi(\omega_o,z_s)\psi(\omega_o,z_{tar})}{\sqrt{k_m^o}}\exp\left(-i\left(\omega_o t-k_m^o r_1\right)\right) \\ \times\exp\left(-\left(t-\frac{\partial k_m}{\partial\omega}r_1\right)^2\left(4\Delta\Omega^{-2}-2i\frac{\partial^2 k_m}{\partial\omega^2}r_1\right)^{-1}\right) \\ \times\left(\pi\left(\Delta\Omega^{-2}-i\frac{1}{2}\frac{\partial^2 k_m}{\partial\omega^2}r_1\right)^{-1}\right)^{1/2} \end{aligned} \tag{18}$$

where

$$\Omega^2=\begin{cases} \infty & uniform \\ 2\Delta\omega^2 & Gaussian. \\ i2(\omega_1-\omega_2)/T & LFM \end{cases} \tag{19}$$

3.2.2 Two-way target response in a shallow water waveguide

The computation of the target response entails the convolution of the two one-way Greens functions from the source to the target and from the target to the receiver with each other and with the impulse response *ts* of the target itself

$$p_{target}(t)=\int_{-\infty}^{\infty}p\left(t-\tau_1,\mathbf{r}_{tar},z_{tar}\middle|\mathbf{r}_{rec},z_{rec}\right)\int_{-\infty}^{\infty}ts(\tau_1-\tau_2,\varphi_s,\varphi_{rec})\,p\left(\tau_2,\mathbf{r}_s,z_s\middle|\mathbf{r}_{tar},z_{tar}\right)d\tau_2 d\tau_1 \tag{20}$$

where φ_1 and φ_2 are the azimuthal angles to the source and the receiver in the coordinate system of the target as shown in Fig. 2

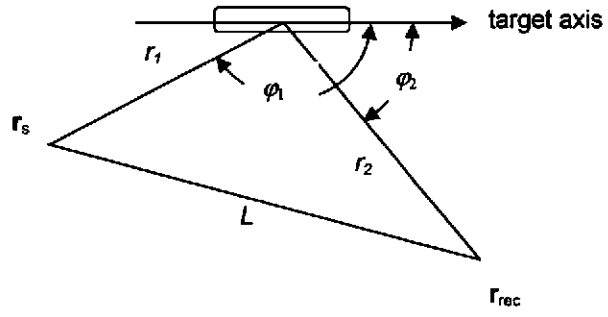

Figure 2: Bistatic target geometry

In (20) the presence of the target is assumed not to change either of the Greens functions. Additionally, the target impulse response is assumed to be indifferent to the directional composition of either of the Greens functions, apart from the assumption that the orientation of the target with respect

to the source and receiver in the horizontal plane is important. These assumptions are most valid for objects which are elongated in the horizontal plane but which are not to large with respect to a wavelength or with respect to the waveguide depth in the vertical plane. The implications of this assumption are that no multiple target-boundary interactions will be included in the calculation of the target response, and no shadowing of the incident or scattered field by the object itself will be included.

Under the assumptions above it remains to define the target response impulse response. The impulse response of interest is the field amplitude radiated into azimuth φ_2 at 1 m by a unit amplitude plane wave incident at azimuth φ_1. Under this definition the target strength *TS* is defined as

$$TS = 10\log 10\left(\left|\tilde{ts}(\omega_o, \varphi_s, \varphi_{rec})\right|^2\right) \tag{21}$$

where $\tilde{ts}$ is the Fourier transform of the target impulse response at the centre frequency of the source pulse. Under the simple spherical scatterer hypothesis, *ts* is not dependent on azimuth, and may be assumed to be a delta function whose strength is determined by a desired target strength

$$ts(t) = 10^{TS/20}\delta(t) \tag{22}$$

in which case (20) reduces to

$$p_{target}(t) = 10^{TS/20}\int_{-\infty}^{\infty} p(t-\tau, \mathbf{r}_{tar}, z_{tar}|\mathbf{r}_{rec}, z_{rec})\, p(\tau, \mathbf{r}_s, z_s|\mathbf{r}_{tar}, z_{tar})\, d\tau \tag{23}$$

4 STIMULATOR IMPLEMENTATION

4.1 Reverberation

At any given time a horizontal line array of *N* elements observes the reverberation intensity across azimuth and grazing angle in *N* discrete wavenumbers according to the relation

$$\begin{aligned}\tilde{p}(k) &= \sum_{n=-N/2}^{N/2-1}\int_{-L/2}^{L/2} p(x)\delta(x-n\delta x)\exp(ikx)\,dx \\ &= \sum_{n=-N/2}^{N/2-1} p(n\delta x)\exp(ikn\delta x)\end{aligned} \tag{24}$$

where at design frequency $\delta x = \lambda/2$, and *L* is the length of the array $L = N\delta x$. For $k = m\delta k$ (12) forms part of the discrete Fourier transform pair

$$\begin{aligned}\tilde{p}[m] &= \sum_{n=-N/2}^{N/2-1} p[n]\exp(i2\pi nm/N) \\ p[n] &= \frac{1}{N}\sum_{n=-N/2}^{N/2-1}\tilde{p}[m]\exp(-i2\pi nm/N)\end{aligned} \tag{25}$$

where $\delta k = 2\pi/L$ such that $kn\delta x = 2\pi nm/N$. Thus the pressure at the *N* hydrophone locations $p[n]$ is completely determined the decomposition of the pressure into the *N* wavenumbers $k = \left[-\frac{N}{2}\delta k, -\frac{\left(\frac{N}{2}-1\right)}{\delta k}, \ldots, \frac{\left(\frac{N}{2}-1\right)}{\delta k}\right]$, when the array is operating at the design frequency.

The intensity of each wavenumber component of the pressure may be determined by summing the square root of the angular density of the reverberation intensity (11) for each as resolved by the finite array aperture

$$\tilde{I}_{rev}(t,[m]) = \int_{-\pi}^{\pi} d\phi \int_{-\theta_c}^{\theta_c} d\theta \quad I_{rev}(t,\theta,\phi)\,\mathrm{sinc}^2\left(kL\left(\cos\theta\cos\phi - m\delta k/k\right)\right) \tag{26}$$

where the square of the **sinc** function represents the product of the resolution function of the finite array aperture with the infinite resolution theoretical intensity distribution I_{rev}.

In Fig. 3 the reverberation intensity as a function of azimuth and grazing angle is shown in the top panel a short time after the direct blast for a bistatic scenario where the source is 10 km from the receiver. In this geometry the azimuthal angle ϕ is zero when pointing towards the source. Note that the reverberation which has scattered from scatterers on the far side of the source suffers significant attenuation on the way to the receiver, as is visible from the limited grazing angle extent of the energy at angles between 350 and 10 degrees azimuth. The array is aligned with the source-receiver axis and an end-fire beam is pointed away from the source: the conical beampattern for this beam is shown in the second panel. In the bottom panel the product of the beam pattern with the azimuthal and grazing angle dependent reverberation intensity is shown. This product is integrated over azimuth and grazing angle to obtain the intensity of the reverberation in coming from the end-fire direction. Similar integrals are performed for the *N+1* wavenumbers corresponding to the resolution of the array at a sampling of times after the direct blast.

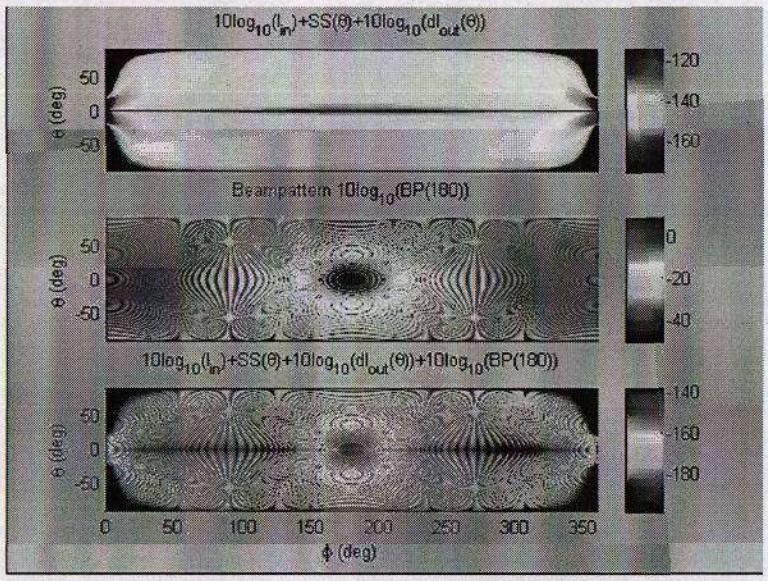

Figure 3: Reverberation intensity as a function of azimuth and grazing angle (top). Conical beampattern of array pointing at end-fire (middle). Product of reverberation intensity and conical beampattern is shown in the bottom panel.

Once the *N+1* slow-time intensities $\tilde{I}_{rev}(t,[m])$ are computed using 26, the fast-time element level reverberation impulse responses are computed by

$$p_{rev}(t,n\delta x) = \sum_{m=0}^{N} \sqrt{\tilde{I}_{rev}(t,[m])}\exp(i2\pi mn/N)\,p_{rand}(t) \tag{27}$$

where $\tilde{I}_{rev}(t,[m])$ has been interpolated to the sample frequency required of the stimulator and the randomized time series $p_{rand}(t)$ is a unity variance Rayleigh envelope distributed (uncorrelated Gaussian quadratures) white random process also sampled at the sample frequency. The element

level impulse response is finally convolved with the source waveform to obtain the final stimulator output.

4.2 Target

As discussed in 2.2.2, the target calculation is accomplished most rapidly for point targets by convolving the two one-way Greens functions between the source and the target and the target and the receiver. For Gaussian pulse shapes, the final source function may be obtained by convolving the two one-way Greens functions where the bandwidth for each has been doubled, taking advantage of the property that the convolution of two Gaussians with equal time duration results in a Gaussian with twice the original duration. This avoids the numerical difficulties associated with convolving a source-target Greens function where the source bandwidth has been included with the target-receiver Greens function, which is by definition of infinite bandwidth and thus composed of the superposition of delta functions which may not fall on the sample times. Thus for a desired end bandwidth of $\Delta\omega$ (23) is implemented where (18) is evaluated with

$$\Omega^2 = \begin{cases} \infty & uniform \\ \Delta\omega^2 & Gaussian \\ i(\omega_1 - \omega_2)/T & LFM \end{cases}. \tag{28}$$

while the target-receiver Greens function is computed using

$$\begin{aligned} p(t, \mathbf{r}_{tar}, z_{tar} | \mathbf{r}_{rec}, z_{rec}) \approx \sqrt{\frac{2\pi}{r_2}} \sum_{n=1}^{N} \frac{\psi(\omega_o, z_s)\psi(\omega_o, z_{tar})}{\sqrt{k_m^o}} \exp\left(-i\left(\omega_o t - k_m^o r_2\right)\right) \\ \times \exp\left(-\left(t - \frac{\partial k_m}{\partial \omega} r_2\right)^2 \left(4/\Delta\omega^{-2} - 2i\frac{\partial^2 k_m}{\partial \omega^2} r_2\right)^{-1}\right) \\ \times \left(\pi\left(\Delta\omega^{-2} - i\frac{1}{2}\frac{\partial^2 k_m}{\partial \omega^2} r_2\right)^{-1}\right)^{1/2} \end{aligned} \tag{29}$$

Note 29 is computed without the normalization factor of $1/2\pi$. This is because the convolution is equated with the frequency domain product of two equations of the form of (16), which requires only one factor of $1/2\pi$.

5 RESULTS

Several reverberation modelling benchmarks were defined at the ONR reverberation modelling workshops (RMW) held in November 2006 and April 2008 at ARL-UT [5] and at the David Weston Memorial Sonar Performance Prediction Symposium (WSPPS) conducted in April 2010 in Cambridge UK [6]. Problem XI from the first ONR workshop asked for reverberation solutions for a monostatic geometry in an isovelocity waveguide with Lambert's law bottom scattering. Problem T from the 2008 ONR workshop asked for the addition of a 5 m radius vacuum sphere target to Problem XI to allow the computation of signal excess (together Problems XI and T are very similar to Scenario A2 from the Weston symposium). The stimulator described herein has been exercised for Problems XI and T at 250, 1000, and 3500 Hz. The environment is shown in Fig. 4 taken from the Reverberation Modelling Workshop website [8]. The sound speed in the water c is 1500 m/s at all depths, with a density ρ of 1.024 g/cm^3. The bottom sound speed c_b is 1700 m/s, with a density ρ_b of 2.048 g/cm^3. The bottom attenuation is 0.5 dB/λ, and the bottom scattering is defined by Lambert's law

$$\begin{aligned} SS(\theta_1,\theta_2,|\phi_2-\phi_1|) &= 10\log 10\left(ss(\theta_1,\theta_2,|\phi_2-\phi_1|)\right) \\ &= -27+10\log 10(\sin\theta_i \sin\theta_s) \end{aligned} \tag{30}$$

The target itself is a 5m radius vacuum sphere deployed at a depth of 10 m at ranges of 2.5, 5, 10, 20 and 40 km. The target strength of this sphere as a function of frequency is shown by the blue curve in Fig. 5, and has a value very close to the geometric optics limit

$$\begin{aligned} TS &= 10\log 10\left(ts(\theta_1,\theta_2,|\phi_2-\phi_1|)\right) \\ &= 20\log 10(a/2) \\ &= 7.96 \quad dB re \quad 1m \end{aligned} \tag{31}$$

over the frequency band of interest. The source depth is 30 m and the receiver depths are 10, 50, and 90 m.

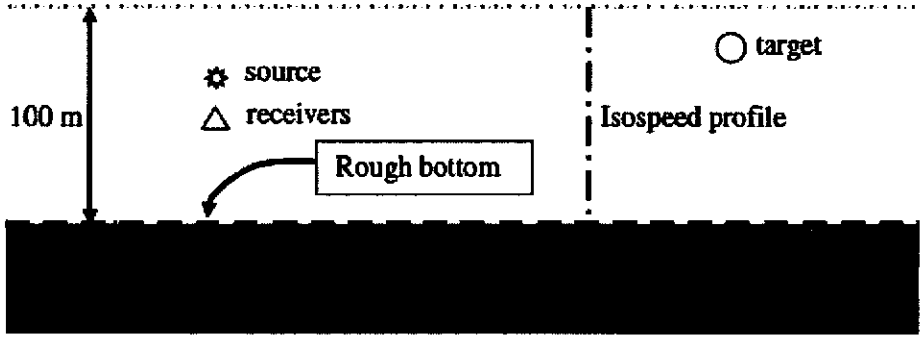

Figure 4: RMW Problem XI+T (WMSPPS Problem A2)

The source waveform specified for the RMW was of the form

$$p(t) = A(\omega_o)\cos(\omega_o t)\exp\left(-(t\Delta\omega)^2/2\right) \tag{32}$$

where $A(\omega_o) \equiv 1$, $\Delta\omega = \omega_o/20$, and $\omega_o = 2\pi f_o$ with f_o being the centre frequency of interest. The source waveform (32) was modified for the WSPPS through the specification of an amplitude A of 73 kPa at $f_o = 250$ Hz, 146 kPa at $f_o = 1$ kHz, and $f_o = 273$ kPa at 3.5 kHz, giving a frequency independent energy source level (*ESL*) of 200 dB re µPa-s, where *ESL* is defined as

$$ESL = 10\log 10\left(\int p^2(t)dt\right) \tag{33}$$

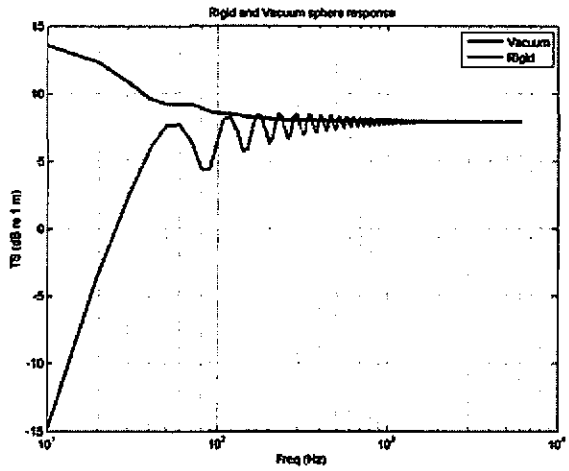

Figure 5: Target strength of a vacuum (blue) and rigid (red) 5 m diameter sphere.

5.1 RMW Problem XI+T (WSPPS Problem A2) 250 Hz

250 Hz results for both the phone level reverberation and the target are shown in Fig. 6. The stimulator results are shown both as a representative single phone level (grey) and the rms average of all phone levels for a half-lambda spaced (3 m) 65 element horizontal array (blue). Also superimposed are some non-stimulator results: the output of the R-SNAP model [9] for the incoherent reverberation intensity at three different receiver depths (10m (blue), 50 m (green), and 90 m (red)) using the workshop source waveform, and the closed form expressions for the reverberation level (RL) (magenta) and the echo level (EL) (cyan) from [4], which assume a linear log reflection coefficient with angle. The RL (black) and EL (grey) for the actual non-linear reflection coefficient are also shown. Finally the amplitude of the complex envelopes of the target responses are shown in blue for ranges of 2.5, 5, 10, 20 and 40 km from the source/receiver position.

Some observations regarding these results may be made. First is that the stimulator results and the R-SNAP results for the RL are very close, although at this low frequency there are some slight differences in the R-SNAP results at the different depths (the stimulator results are independent of depth). The second is that the closed form expressions and the stimulator results for the reverberation and echo level differ due to the highly non-linear reflection coefficient of the bottom specified for this problem. This may be seen in Fig. 7, which shows the reflection coefficient (red) compared with the log-linear approximation (blue). It may be seen that the log-linear reflection significantly overestimates the loss at grazing angles above approximately 6 degrees. This leads to higher losses and therefore lower reverberation and echo levels in the closed form results, especially at early times. The third is that while the closed form expressions have neglected the effects of volume absorption, these effects are negligible at this frequency, and the differences between the various results at long-range are more significantly impacted by whether the actual reflection coefficient or its log-linear approximation are used.

The target results generated by the stimulator for the distinct ranges show a significant amount of structure, and their maximum level is clearly not monotonically decreasing as in the closed form (cyan) or numerically integrated (grey) results. The structure and variable peak amplitude are both caused by multipath.

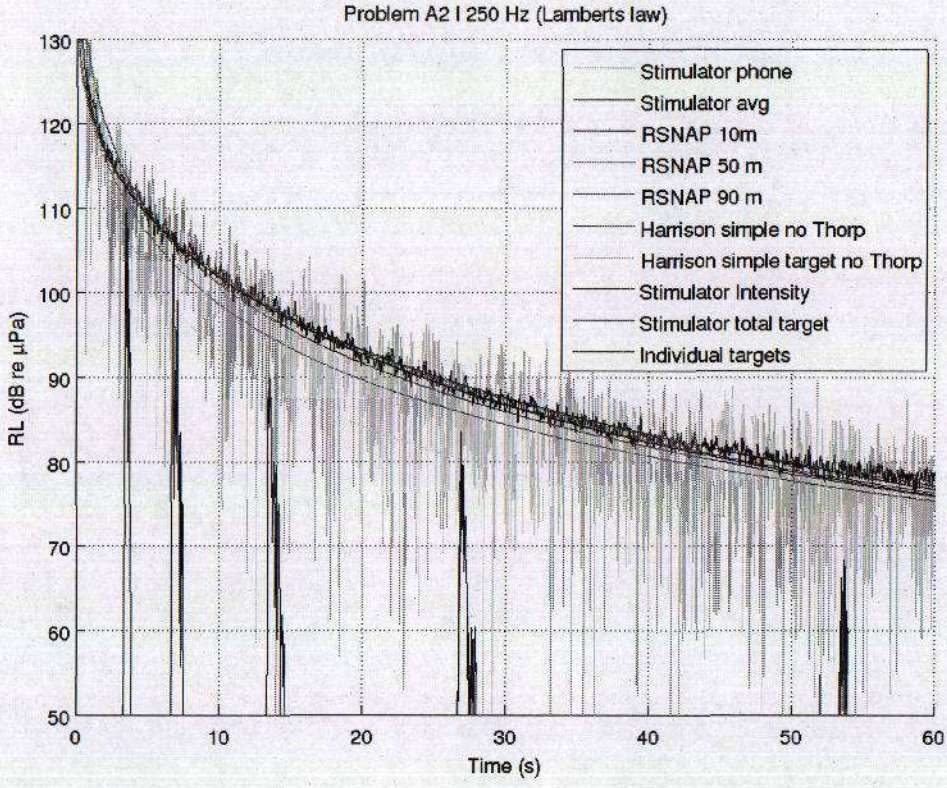

Figure 6: RMW Problem XI + T (WSPPS Scenario A2) reverberation level at 250 Hz.

In Fig. 8 the reverberation and response of a target at 250 Hz for 10 km range are shown on an expanded scale. The target response is elongated in time by 1.78 s due to multipath dispersion which is limited by the critical angle, and has roughly an exponential decay for the first 0.89 s as discussed in [7]. The strong fading of the target response as a function of time is due to the precise location of the source, receiver and target in the waveguide. The agreement between the closed form expressions for the target response (cyan) and the stimulator time series is unusual as inspection of Fig. 6 shows.

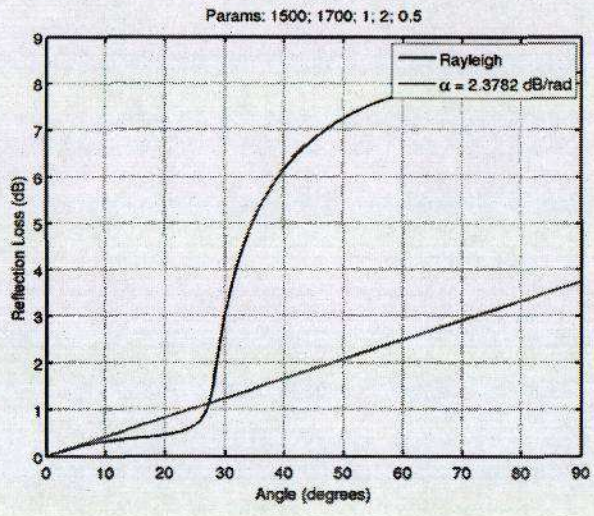

Figure 7: Rayleigh reflection coefficient and Weston log-linear approximation for workshop bottom

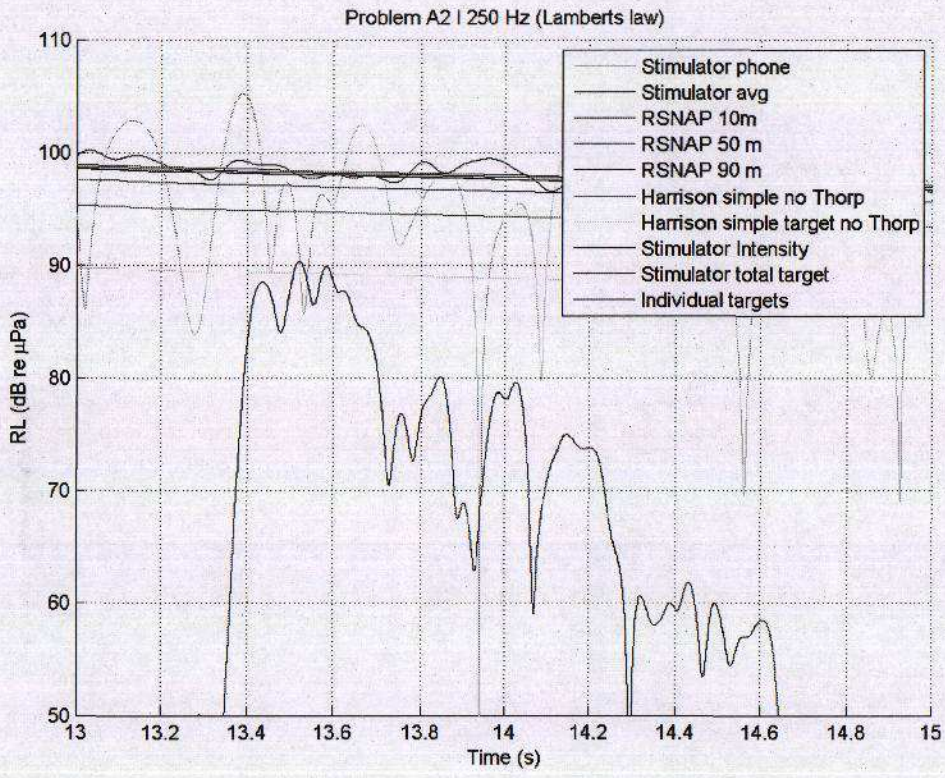

Figure 8: 10 km target response and reverberation for RMW Problem XI + T (WSPPS Scenario A2) at 250 Hz.

5.2 RMW Problem XI+T (WMSPPS Problem A2) 1 kHz

Various results for 1 kHz are shown in Fig. 9. The levels of the reverberation are similar to the results at 250 Hz for times less than about 5 s, due to the identical ESL of the source pulse at the two frequencies (RL is linear in ESL). However, the levels at greater times are lower for the 1 kHz case due to the effects of volume absorption. As in the 250 Hz case, a representative single phone level is shown in grey, while the averaged result is shown in blue. The incoherent R-SNAP predictions for the three receiver depths are shown by the smooth blue, green, and red curves. As opposed to the 250 Hz results, the 1 kHz results are practically identical for all three receiver depths. The closed form curves for the reverberation and the target response without volume attenuation are superimposed in the magenta and cyan curves, while the numerically integrated curves using the actual reflection coefficient shown in Fig. 7 are shown by the smooth black and grey curves. Comparison between the closed form solutions and the numerically integrated ones shows that the effect of volume attenuation is greater than 5 dB at 60 s, while as in the 250 Hz case the overall levels of the closed form solution are lower at early time (times less than about 20 s) due to the over-estimation of the reflection loss at high grazing angles when using the log-linear approximation.

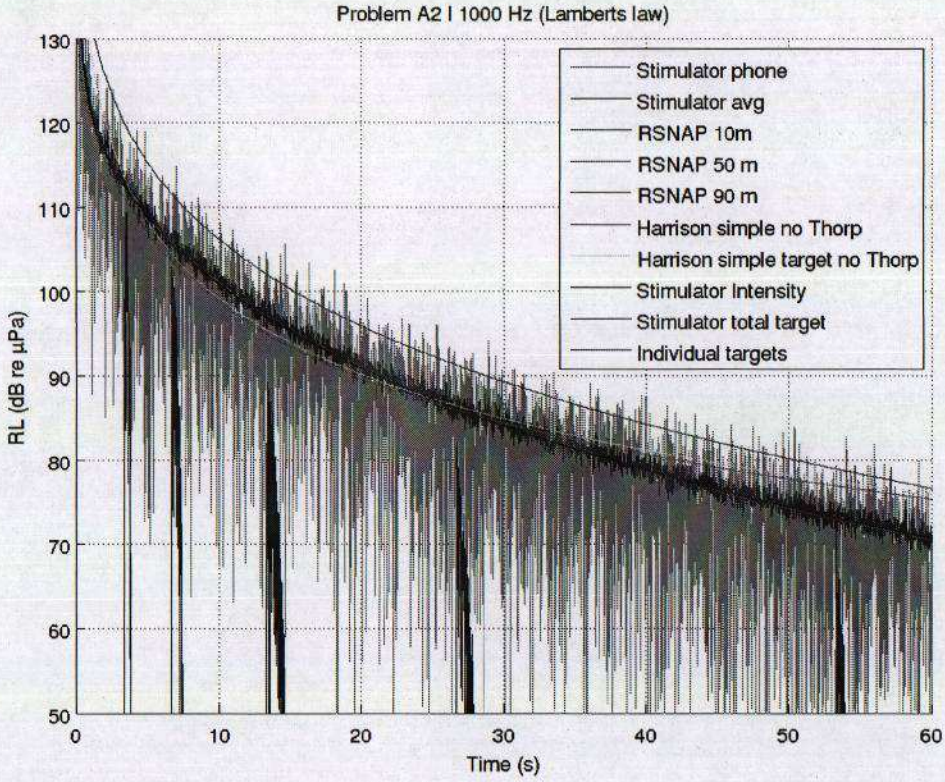

Figure 9: RMW Problem XI + T (WSPPS Scenario A2) reverberation level at 1 kHz.

Also shown in Fig. 9 and in more detail for the 10 km target in Fig. 10 are the target responses. While the identical ESL ensures that the reverberation level is independent of frequency (other than the effects of increasing volume absorption with frequency), the higher peak level of the source pulse at 1 kHz (twice the amplitude of the 250 hz pulse) yields roughly 6 dB higher echo levels for the target. As in the 250 Hz case, the target responses do not show a uniform decrease in level as a function of time, due to the continued importance of multipath interference effects. For instance, the return for the 10 km target seems to suffer anomalously high loss (low echo level), while that for the 20 km target is conversely anomalously low (high echo level). This can be seen by comparing the level of the target returns to the background reverberation. The target at 20 km seems to have a 4 dB signal to reverberation ratio (SRR), while the 10 km target has a just slightly more than 10 dB SRR. Even more striking, the targets at 2.5, 5, and 40 km have SRRs of between -3 and 0 dB.

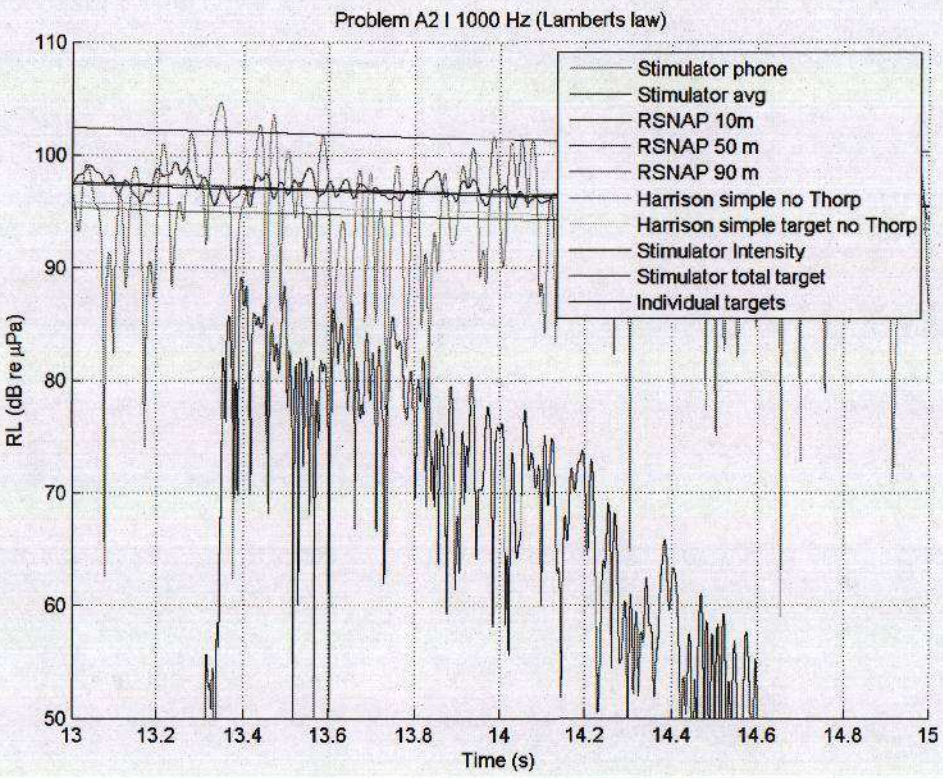

Figure 10: 10 km target response and reverberation for RMW Problem XI + T (WSPPS Scenario A2) at 1 kHz.

As in the 250 Hz case, the decay of the target return at 10 km at 1 kHz is roughly exponential for the first 0.89 s after the first arrival (13.33-14.22 s, 14.22 s being equal to the round trip travel time of 13.33 s plus the one-way pulse dispersion time τ_c from Eq. 4 in [7], for $\theta \equiv a\cos(c/c_b)$), while it falls off at a more rapid rate between 14.22 and 15.11 s as given by Eq. 9 of [7]. As in the 250 Hz example, the multipath interference effects are clearly visible in the high variability of the envelope as a function of time. However, as the bandwidth for the 1 kHz case is 25% of the 250 Hz bandwidth, the multipath are more clearly resolved.

5.3 RMW Problem XI+T (WMSPPS Problem A2) 3.5 kHz

The RL and SL results for 3.5 kHz are shown in Fig. 11. The EL levels are again higher than in the previous results due to the higher peak level of the source waveform (5.4 dB higher than the 1kHz example and 11.4 dB higher than in the 250 Hz case) while the RL stays essentially the same until the higher volume attenuation becomes apparent at times beyond approximately 2 s. At 60 s the RL is only 56 dB re µPa, as compared to 70 dB re µPa at 1 kHz and 77 dB re µPa at 250 Hz. This is consistent with the form of the volume attenuation formula used [10]

$$\alpha_w(f) = 3.3\times10^{-3} + \frac{0.11f^2}{1+f^2} + \frac{44f^2}{4100+f^2} + 3.0\times10^{-4} f^2 \qquad (34)$$

where f is the frequency in kHz and the attenuation units are dB per km.

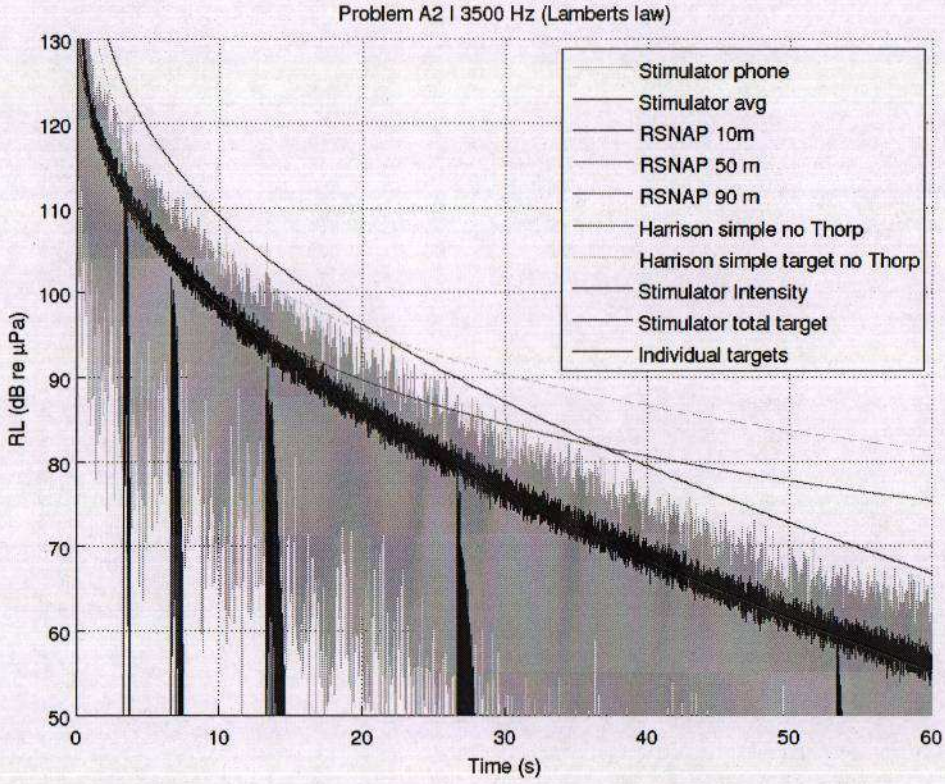

Figure 11: RMW Problem XI + T (WSPPS Scenario A2) reverberation level at 3.5 kHz.

Also evident in Fig. 10 is the very good agreement between the phone-averaged stimulator results shown in blue and the R-SNAP results obtained from normal mode theory.

In Fig. 12 the results in the vicinity of the target return from the 10 km target are shown. The bandwidth of 175 Hz resolves many of the multipath, causing the target to have a very high amplitude variance as a function of time. As in the lower frequency results, the target decays exponentially for the first 0.89 s.

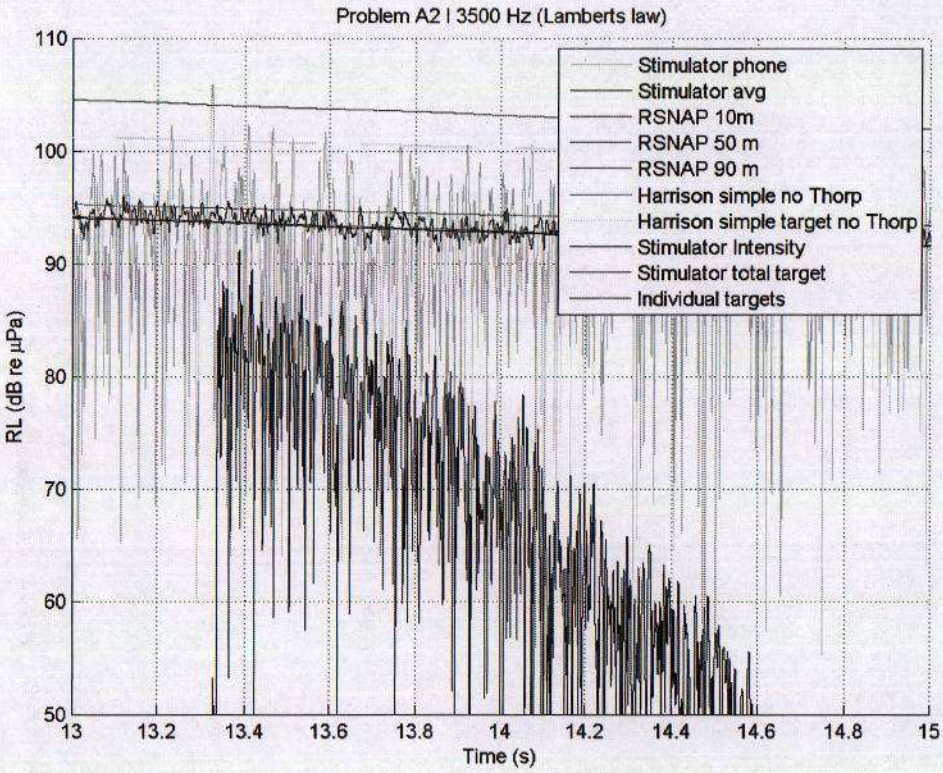

Figure 12: 10 km target response and reverberation for RMW Problem XI + T (WSPPS Scenario A2) at 3.5 kHz.

6 CONCLUSIONS

A fast sonar stimulator has been developed based on the ray-averaged or energy flux expressions for reverberation developed by Weston and Harrison. The resulting code has been run for the sonar scenario A2 from the David Weston Memorial Sonar Performance Prediction Symposium. A time-domain normal-mode target response simulation based on normal mode theory has also been exercised for these scenarios. RL results compare favourably to those predicted by the R-SNAP normal-mode based reverberation model. The stimulator is capable of generating time-domain element level reverberation and target time series on horizontal line arrays in real time on a desktop computer. The resulting time series may be beamformed and processed like real data for in-the-loop sonar simulation scenarios for training, algorithm development, or testing autonomy algorithms for autonomous assets such as AUVs towing line arrays.

The key to the efficiency of the approach is the decomposition of the reverberation intensity into the $N+1$ distinct wavenumber components resolved by a straight, uniformly spaced line array operating at the design frequency. For this type of receiver, the conical beampatterns in azimuth and grazing angle may be readily calculated and products of these beampatterns with the background slow-time evolving reverberation intensity densities may be integrated to give $N+1$ independent intensities resolved by the array. The square root of these intensities may then randomized and summed to give the reverberation impulse response. As opposed to methods where the scattered field computed by large numbers of scatterers are summed, such an approach is extremely efficient. In addition, the use of simple expressions derived by Harrison for the time evolution of the bistatic reverberation intensity in waveguides as a function of azimuth and grazing angle further increases the efficiency of the stimulator.

A normal-mode based target stimulator to compliment the flux theoretic reverberation stimulator has also been presented. Fully coherent and explicitly in the time domain, the target stimulator is able to rapidly and accurately calculate the target return for simulating reverberation plus target sonar

scenarios. The key to the efficiency of the target stimulator is the use of the narrow-band approximation, which makes it possible to Fourier transform the frequency-domain normal mode expressions for the return from a target analytically. Together, the reverberation and the target stimulation tools comprise a new real-time stimulation capability for mid-frequency sonar at tactical ranges.

7 REFERENCES

1. R. Been, D.T. Hughes, J.R. Potter, and C. Strode, 'Cooperative anti-submarine warefare at NURC: moving towards a net-centric capability', Proc. IEEE OCEANS 2010, Sidney (2010).
2. K.D. LePage, 'An SNR maximization behaviour for autonomous AUV control', Proc. 10th European Conf. on Underwater Acoustics, Istanbul (2010).
2. D.T. Hughes, S. Kemna, M. Hamilton and R. Been, 'Sensible behaviour strategies for AUVs in ASW scenarios', Proc. IEEE OCEANS 2010, Sidney (2010).
3. C.H. Harrison, 'Formulae for bistatic signal and reverberation' SACLANTCEN SR-371. La Spezia, Italy, NATO SACLANT Undersea Research Centre, 2002
4. ONR Reverberation Modelling Workshop I, Pickle Research Centre, ARL-UT November 2006.
5. David Weston Memorial Sonar Performance Prediction Workshop, Clare College, Cambridge, UK, April 2010.
6. C.H. Harrison and P.L. Nielsen, 'Multipath pulse shapes in shallow water: Theory and simulation', J.Acoust.Soc.Am. 121(3) 1362-1373 (2007).
7. ftp://ftp.ccs.nrl.navy.mil/pub/ram/RevModWkshp_II/Workshop_1_Problem_ Definitions/Reverb_Workshop_I_Problem_Diagrams.pdf last accessed 26 April 2010.
8. K.D. LePage, 'Bottom reverberation in shallow water: Coherent properties as a function of bandwidth, waveguide characteristics, and scatterer distributions', J.Acoust.Soc.Am. 106(4) 3240-3254 (1999).
9. W.H. Thorp, 'Analytic description of the low-frequency attenuation coefficient', J.Acoust.Soc.Am. 42(1) 270 (1967).